

Patient-Specific Orthotopic Glioblastoma Xenograft Models Recapitulate the Histopathology and Biology of Human Glioblastomas In Situ

Kyeung Min Joo,^{1,5,10} Jinkuk Kim,^{5,6,10} Juyoun Jin,^{2,10} Misuk Kim,^{2,10} Ho Jun Seol,^{2,10} Johongir Muradov,² Heekyoung Yang,² Yoon-La Choi,³ Woong-Yang Park,⁴ Doo-Sik Kong,² Jung-Il Lee,² Young-Hyeh Ko,^{3,5} Hyun Goo Woo,⁷ Jeongwu Lee,⁸ Sunghoon Kim,⁹ and Do-Hyun Nam^{2,5,*}

¹Department of Anatomy and Cell Biology

²Department of Neurosurgery

³Department of Pathology

⁴Samsung Genome Institute

Samsung Medical Center, Sungkyunkwan University School of Medicine, Seoul, 135-710, Korea

⁵Samsung Biomedical Research Institute, Seoul, 135-710, Korea

⁶Samsung Advanced Institute of Technology, Samsung Electronics, Seoul, 137-857, Korea

⁷Department of Physiology, Ajou University School of Medicine, Suwon, 443-721, Korea

⁸Department of Stem Cell Biology and Regenerative Medicine, Lerner Research Institute, Cleveland Clinic, Cleveland, OH 44195, USA

⁹Medicinal Bioconvergence Research Center, Department of Molecular Medicine and Biopharmaceutical Sciences, Seoul National University, Seoul, 151-742, Korea

¹⁰These authors contributed equally to this work

*Correspondence: nsnam@skku.edu

<http://dx.doi.org/10.1016/j.celrep.2012.12.013>

SUMMARY

Frequent discrepancies between preclinical and clinical results of anticancer agents demand a reliable translational platform that can precisely recapitulate the biology of human cancers. Another critical unmet need is the ability to predict therapeutic responses for individual patients. Toward this goal, we have established a library of orthotopic glioblastoma (GBM) xenograft models using surgical samples of GBM patients. These patient-specific GBM xenograft tumors recapitulate histopathological properties and maintain genomic characteristics of parental GBMs in situ. Furthermore, in vivo irradiation, chemotherapy, and targeted therapy of these xenograft tumors mimic the treatment response of parental GBMs. We also found that establishment of orthotopic xenograft models portends poor prognosis of GBM patients and identified the gene signatures and pathways signatures associated with the clinical aggressiveness of GBMs. Together, the patient-specific orthotopic GBM xenograft library represent the preclinically and clinically valuable “patient tumor’s phenocopy” that represents molecular and functional heterogeneity of GBMs.

INTRODUCTION

Glioblastoma (GBM) is the most common and lethal primary brain tumor. Aggressive standard-of-care therapy including

concurrent chemoradiation treatment based on the oral methylator temozolomide (TMZ) and more recent molecular-targeted therapeutics provide only palliation, unable to change the near uniform lethality of this disease (Adamson et al., 2009; Chi and Wen, 2007; Furnari et al., 2007). However, differential responses of GBM patients to the TMZ-based chemotherapy has been recognized and it is now believed that therapeutic benefit by TMZ is much greater in a cohort of GBMs with low expression of O6-methylguanine-DNA methyl transferase (MGMT) (Hegi et al., 2005; Stupp et al., 2005). This prototypic example highlights the importance of molecular and genetic GBM heterogeneity in the development of novel therapeutics and companion diagnostics (Nicholas et al., 2011).

Traditionally, preclinical cancer biology has largely relied on the use of human cancer cell lines in vitro and the xenograft tumor models derived from these cell lines. However, the process of establishing conventional GBM cell lines results in irreversible loss of important biological properties and, as a result, the xenograft tumor models do not maintain genomic and phenotypic characteristics present in the original tumor (Martens et al., 2008; Sausville and Burger, 2006; Taillandier et al., 2003). More importantly, loss of specific properties of individual tumors induces the failure to represent the GBM heterogeneity (Bonavia et al., 2011; Lee et al., 2006; Verhaak et al., 2010). Therefore, it is questionable whether those preclinical platforms can serve as a reliable “filter” to select the lead candidate compounds or “tester” to determine the therapeutic efficacy of drugs.

It has been postulated that in vitro and in vivo preclinical models using primarily cultured GBM cells recapitulate the biology of the disease more precisely (Lee et al., 2006; Xie et al., 2008). However, it is still controversial whether those translational models would be functionally better, because thorough

preclinical and clinical validation of the platform using comparable GBM patient population and corresponding animal models has not been addressed yet. Here, we report the establishment of the matched *in vitro* and *in vivo* GBM model systems that are derived from patient specimens. We provide evidence that this preclinical model recapitulate the biology of human GBM *in situ*, and precisely verified their preclinical and clinical implications.

RESULTS

In Vitro Cultures and Orthotopic Xenograft Tumor Models

Seventy-one surgical specimens (Table 1; Figure S1) were collected from 59 GBM patients (from 11 patients, both primary and recurrent tumor specimens were acquired; from one patient, two recurrent specimens with no primary sample were acquired). We dissociated GBM cells from each specimen and stereotactically injected into the brains of immune-compromised NOD/SCID *Il2rg*^{-/-} (NOG) mice (Ito et al., 2002) within 12 hr after surgery. In parallel, *in vitro* growth kinetics of the freshly isolated GBM cells were determined by culturing them in serum-free media in the presence of EGF and bFGF (Joo et al., 2008). Because clonogenic growth as neurospheres is an *in vitro* indicator of self-renewal in GBM stem cells, we used sphere formation (diameter $\geq 50 \mu\text{m}$) as the readout for *in vitro* growth of GBMs. *In vivo* tumorigenicity was defined as the formation of tumor within 12 months after tumor cell injection. Due to technical issues including the limited number of cells available, we could not test one sample for *in vivo* tumorigenic potential and 21 samples for *in vitro* sphere formation capacity (Table 1; Figure S1).

With this paralleled *in vivo* xenograft tumors and *in vitro* short-term cultures, we determined a potential correlation between the two. *In vivo* xenograft tumor formation was histopathologically confirmed in 53 cases from 70 samples (75.7%) (Table 1; Figures 1A and S1A). Robust *in vitro* sphere formation and sustained growth was confirmed in 34 cases from 50 samples (68.0%) (Table 1; Figures 1A and S1B). There appeared to be a positive correlation; however, it was not statistically significant (Fisher's exact test, $p = 0.09$; Figure 1B).

In Vivo Tumorigenicity and Clinical Aggressiveness of Parental Tumors

Both *in vitro* primary cultures and orthotopic xenograft tumor models are the crucial parts of preclinical evaluation platform for new anticancer therapeutics. We reasoned that the readouts of an adequate platform should be able to represent pathoclinical parameters of patients. With this notion, we correlated the *in vitro* growth or xenograft tumor formation with the clinical information of the GBM patients. Progression free survival (PFS) and overall survival (OS) of the patients were utilized as indicators of GBM aggressiveness. Clinical data of primary GBMs ($n = 58$) was utilized for survival analysis, from which PC-NS08-532 and IRCR-GBM10-022 were excluded due to mortality derived from the pulmonary embolism and follow-up loss, respectively (Table 1; Figures S1A and S1B).

In a subset of GBMs with robust *in vitro* sphere formation (Figure S1B, $n = 29$), PFS and OS were 40.0 (28.1–51.9) weeks and

73.0 (53.4–92.6) weeks (median [95% confidence interval]), respectively. The PFS and OS were not statistically different from those of the other group (Figure S1B, $n = 15$, PFS = 44.0 [33.3–54.7] weeks [$p = 0.815$], OS = 82.0 [58.0–106.0] weeks [$p = 0.380$]), suggesting that *in vitro* sphere formation cannot portend the patient survival (Figure S2A). A previous study has reported that adherent cultures using laminin as a cohesive substrate could improve the survival and growth of GBM cells compared to the sphere culture (Pollard et al., 2009). We cultured 17 different GBM cells using both conditions. However, overall growth patterns of the two primary cultures were indistinguishable (Figure S2C). Therefore, it is unlikely that the apparent lack of correlation between *in vitro* growth and the patient survival is due to the use of inadequate *in vitro* culture condition.

In contrast, *in vivo* tumor formation capacities of dissociated GBM cells appeared to correlate with worse clinical outcome (GBMs with tumor formation capacity: $n = 40$, PFS = 41.0 [32.5–49.5] weeks, OS = 71.0 [54.7–87.3] weeks versus GBMs without the capacity: $n = 16$, PFS = 53.0 [40.4–65.6] weeks [$p = 0.075$], OS = 82.0 [76.2–87.8] weeks [$p = 0.303$]), although the trend fell short of statistical significance (Figures 1C and S1A). There was no significant correlation between the *in vivo* tumorigenic potential and other clinical factors such as sex, age, location of lesion, and initial KPS (data not shown; Table 1).

Next, we examined the growth pattern of the patient-derived tumors. Many of xenograft GBM tumors revealed a highly invasive and infiltrative tumor growth pattern, whereas the other xenograft tumors revealed a clear demarcation (Figure 2A). Invasive GBM growth is a major culprit for lethality because it makes complete surgical resection of the tumor impossible. Considering the profound clinical implication of the invasiveness, we classified the primary GBM patients into two groups: (1) GBMs that generated invasive tumor in mouse brains ($n = 27$), and (2) GBMs that failed to make tumor or made well-demarcated tumors ($n = 29$; Table 1; Figure S1A). When PFS and OS of these two groups were compared (Figure S2B), the former group showed a significantly shorter OS (64.0 [59.3–68.7] weeks) than the latter group (99.0 [38.7–159.3] weeks, $p < 0.001$). PFS was also significantly different between these groups (39.0 [34.0–44.0] weeks versus 54.0 [36.6–71.4] weeks, $p = 0.013$). Together, these data suggest that an invasive tumor growth pattern of orthotopic xenograft tumors is a prognostic factor to predict the clinical outcomes of parental GBMs.

Morphologic and Pathologic Similarity

The utility of orthotopic GBM xenografts as a model system of human GBM *in situ* would be greatly increased if xenograft tumors precisely reflect morphologic and pathologic characteristics of their parental tumors. To test, we compared three key parameters in GBM growth and progression; invasiveness, proliferation index, and vessel intensity (Figure S1A):

- (1) Invasiveness (Figures 2A and S3): the invasiveness of each parental tumor was analyzed using MRI T2/FLAIR images according to the response assessment in neuro-oncology (RANO) criteria (Lutz et al., 2011), and a numerical score for invasiveness was allocated comparing

Table 1. Summary of the Clinical Data of GBM Patients and Experimental Results Derived from Primarily Cultured GBM Cells

Clinical Data																	Experimental Data					
Pt. No.	Exp. ID*	Sex	Age	Pathology (Grade)	Ini. KPS	Tx		MRI Finding				PFS (Wk)	OS (Wk)	Status	Subtype	Sphere Form. ^b	In Vivo			PCNA LI	MVD	Gene Exp.
						Rad. Surg.	CCRT	Tumor Size	C/L Inv.	Invas. ^a	Ki67 LI						MVD	Form. ^c	Invas. ^d			
1	P07-428	M	29	GBM (IV)	90	Y	Y	3.1 × 1.8	N	2	12.3	53	84	133	1	P	ND	N	—	—	—	Y
2	P07-436	F	56	GBM (IV)	40	Y	Y	5.4 × 4.2	N	3	45.0	43	34	77	1	C	Y	Y	Y	87.6	40	Y
3	P07-437	F	58	GBM (IV)	90	Y	Y	6.0 × 5.0	N	1	32.7	19	30	71	1	C	N	Y	Y	80.5	41	Y
	P08-559			R-GBM (IV)						3	15.0	38			P	Y	Y		10.6	53	Y	
4	P07-448	M	48	GBM (IV)	90	Y	Y	5.8 × 4.0	N	2	12.2	8	13	13	1	UD	Y	Y	Y	6.9	23	Y
5	P07-453	M	39	GBM (IV)	90	Y	Y	6.8 × 6.7	N	2	5.0	52	122	170	1	P	Y	N	—	—	—	Y
6	P07-458	M	51	GBM (IV)	90	Y	Y	4.9 × 3.2	N	1	73.7	11	56	149	1	M	ND	Y	N	93.3	26	Y
	P08-594			R-GBM (IV)						1	67.3	16			M	ND	Y		89.7	40	Y	
7	P07-460	F	32	GBM (IV)	90	Y	Y	5.9 × 4.9	N	1	74.0	17	49	110	1	UD	ND	Y	Y	86.0	17	Y
	P08-568			R-GBM (IV)						2	50.7	7			N	Y	Y		88.0	37	Y	
8	P07-464	M	59	GBM (IV)	60	Y	Y	6.3 × 4.9	N	1	7.5	16	120	184	1	P	Y	Y	N	7.2	18	Y
9	P07-466	M	36	GBM (IV)	80	Y	Y	5.7 × 5.0	Y	3	20.0	12	41	50	1	P	ND	Y	Y	48.2	19	Y
10	P08-492	F	44	GBM (IV)	80	Y	Y	4.0 × 3.0	N	1	6.8	12	214	214	0	M	Y	N	—	—	—	Y
11	P08-493	M	49	GBM (IV)	90	Y	Y	4.0 × 2.0	Y	3	19.2	27	40	64	1	P	Y	Y	Y	13.9	31	Y
12	P08-496	F	28	GBM (IV)	80	Y	Y	5.5 × 3.5	Y	3	7.5	35	4	82	1	P	N	N	—	—	—	Y
13	P08-498	M	68	GBM (IV)	70	Y	Y	5.5 × 5.0	N	1	38.0	42	64	64	1	P	Y	N	—	—	—	Y
14	P08-503	F	64	GBM (IV)	60	Y	Y	4.6 × 5.2	N	2	1.4	39	71	99	1	C	N	N	—	—	—	Y
15	P08-531	F	71	GS (IV)	70	Y	Y	4.5 × 3.0	Y	1	68.0	18	40	40	1	M	ND	Y	Y	85.3	38	Y
16	P08-532	M	60	GBM (IV)	80	Y	Y	2.5 × 2.0	N	2	1.0	16	4	4	1	C	Y	Y	Y	68.0	37	Y
17	P08-538	F	37	GBM (IV)	80	Y	Y	4.5 × 4.5	N	1	15.5	8	82	195	0	M	Y	Y	N	82.0	20	Y
	P09-773			R-GBM (IV)						2	28.0	9			M	ND	Y	N	96.0	15	Y	
18	P08-541	F	69	GBM (IV)	80	Y	Y	4.5 × 3.0	N	1	13.8	38	39	157	1	C	N	Y	Y	16.1	25	Y
19	P08-543	F	44	GBM (IV)	90	Y	Y	4.0 × 3.5	N	3	1.0	39	44	184	0	M	N	N	—	—	—	Y
20	P08-558	F	45	GBM (IV)	90	Y	Y	5.5 × 4.0	N	1	4.0	22	146	191	0	ND	N	N	—	—	—	N
21	P08-567	F	65	GBM (IV)	80	N	N	3.2 × 2.3	N	3	37.1	19	39	-	2	M	ND	Y	Y	71.4	23	Y
	P09-732			R-GBM (IV)						3	2.0	8			M	ND	Y	Y	6.5	ND	Y	
22	P08-570	F	60	GBM (IV)	80	Y	Y	5.0 × 3.4	N	3	33.5	13	23	24	1	ND	ND	Y	Y	94.0	22	N
23	P08-577	F	62	GBM (IV)	60	Y	Y	5.7 × 3.6	Y	2	59.3	12	34	45	1	M	Y	Y	Y	77.3	13	Y
	P09-680			R-GBM (IV)						3	88.0	ND			N	N	ND	—	—	—	Y	
24	P08-578	M	68	GBM (IV)	90	N	Y	4.0 × 3.0	N	2	37.1	25	67	73	1	P	Y	Y	Y	11.3	12	Y
25	P08-580	F	46	GBM (IV)	70	Y	Y	3.1 × 2.1	N	2	25.7	19	22	71	1	ND	ND	Y	N	ND	ND	N
26	P08-585	M	22	GBM (IV)	90	Y	Y	3.2 × 2.7	N	2	20.4	47	54	123	1	N	N	N	—	—	—	Y
	P09-663			R-GBM (IV)						2	48.7	9			M	ND	Y	N	22.7	7	Y	

Table 1. Continued

Pt. No.	Clinical Data															Experimental Data						
	Exp. ID*	Sex	Age	Pathology (Grade)	Ini. KPS	Tx		MRI Finding				PFS (Wk)	OS (Wk)	Status	Subtype	Sphere Form. ^b	In Vivo		PCNA LI	MVD	Gene Exp.	
						Rad. Surg.	CCRT	Tumor Size	C/L Inv.	Invas. ^a	Ki67 LI						MVD	Tumor Form. ^c				Invas. ^d
27	P08-586	M	40	GBM (IV)	80	Y	N	5.2 × 4.2	N	1	23.3	10	11	28	1	P	N	Y	N	74.7	17	Y
	P09-647			R-GBM (IV)						1	82.0	1			P	ND	Y	N	47.3	6	Y	
28	P08-592	M	44	GBM (IV)	90	Y	Y	4.5 × 2.5	N	2	75.3	8	29	64	1	M	Y	Y	Y	83.3	13	Y
	P09-660			R-GBM (IV)						3	7.2	56			M	Y	Y	Y	3.4	31	Y	
29	P08-608	F	43	GBM (IV)	80	Y	N	2.6 × 2.7	N	1	62.0	13	88	144	1	P	N	Y	Y	86.7	35	Y
30	P08-609	M	48	GBM (IV)	90	Y	Y	4.5 × 3.0	N	1	53.6	41	45	82	1	M	Y	Y	Y	86.7	35	Y
31	P09-626	M	67	GBM (IV)	90	Y	Y	7.5 × 5.0	N	1	5.2	35	79	88	1	C	Y	Y	N	19.1	39	Y
32	P09-630	F	44	GBM (IV)	60	Y	N	4.4 × 2.8	N	3	14.6	12	8	53	1	P	N	Y	Y	10.3	18	Y
33	P09-631	F	53	GBM (IV)	90	Y	Y	5.5 × 3.5	N	1	1.0	16	14	82	1	N	N	N	—	—	—	Y
34	P09-633	F	36	GBM (IV)	80	Y	N	4.0 × 3.0	N	1	6.7	17	119	270	0	N	N	Y	N	22.3	17	Y
35	P09-671	F	47	GBM (IV)	90	Y	Y	6.6 × 4.1	N	3	73.3	5	29	48	1	P	Y	Y	Y	88.0	18	Y
	P09-740			R-GBM (IV)						3	ND	ND			N	Y	N	—	—	—	Y	
36	P09-672	F	76	GBM (IV)	90	Y	Y	4.0 × 3.0	N	3	54.0	9	12	12	1	M	N	N	—	—	—	Y
37	P09-676	M	51	R-GBM (IV)	70	Y	N	2.3 × 1.8	N	1	34.3	13	-	-	0	ND	ND	Y	N	73.3	8	N
	P09-723			R-GBM (IV)						2	26.7	52			M	ND	Y	N	62.1	ND	Y	
38	P09-690	M	57	GBM (IV)	90	Y	Y	5.5 × 5.0	N	3	16.4	17	36	61	1	P	Y	Y	Y	72.6	24	Y
39	P09-696	M	70	GBM (IV)	50	Y	Y	4.8 × 3.1	N	3	3.9	22	54	54	1	C	N	Y	Y	25.6	28	Y
40	P09-705	M	67	GBM (IV)	70	Y	Y	2.8 × 2.2	N	3	50.0	9	34	51	1	ND	Y	N	—	—	—	N
41	P09-727	M	61	GBM (IV)	90	Y	Y	5.0 × 3.4	N	2	40.0	15	38	80	1	M	N	Y	N	82.3	20	Y
42	P09-745	M	58	GBM (IV)	70	Y	Y	3.9 × 3.8	N	2	15.2	15	17	102	1	C	Y	Y	Y	63.3	30	Y
43	P09-748	M	51	GBM (IV)	70	Y	Y	6.5 × 4.5	Y	3	30.0	40	40	40	0	P	Y	Y	Y	45.3	34	Y
44	P09-751	F	46	GBM (IV)	60	N	Y	4.4 × 3.4	N	3	17.1	21	54	87	1	M	Y	Y	Y	54.0	31	Y
45	P09-763	M	66	GBM (IV)	70	Y	Y	3.1 × 2.6	N	2	21.0	16	49	59	1	ND	ND	Y	Y	54.2	ND	N
46	P09-776	M	58	GBM (IV)	70	Y	Y	5.3 × 4.8	N	3	20.2	24	50	63	1	ND	ND	N	—	—	—	N
47	P09-780	M	74	GBM (IV)	40	Y	Y	6.6 × 3.6	N	2	30.0	21	24	65	1	P	Y	Y	Y	67.2	32	Y
	I10-025			R-GBM (IV)						3	32.1	17			M	ND	Y	N	41.2	24	Y	
48	P09-788	M	62	GBM (IV)	60	Y	Y	5.8 × 5.4	N	3	16.5	9	53	56	1	ND	ND	N	—	—	—	N
49	I10-011	F	30	GBM (IV)	60	N	Y	4.7 × 2.8 3.6 × 1.7	N	2	41.8	29	69	89	0	C	Y	Y	N	75.5	36	Y
50	I10-016	M	67	GBM (IV)	60	Y	Y	6.7 × 6.1	N	2	79.3	10	37	60	1	C	Y	Y	Y	81.2	16	Y
51	I10-022	M	63	GBM (IV)	40	N	Y	6.0 × 3.2	N	3	30.0	20	-	-	2	P	ND	Y	Y	83.5	43	Y
52	I10-023	M	31	GBM (IV)	90	Y	Y	5.0 × 3.7	N	1	50.0	11	64	89	0	C	ND	Y	N	83.2	19	Y
53	I10-029	F	50	GBM (IV)	80	Y	Y	3.5 × 2.4	N	2	16.7	14	38	63	1	ND	Y	N	—	—	—	N
54	I10-042	M	49	GBM (IV)	90	N	Y	4.5 × 3.2	N	3	11.8	21	37	79	1	ND	Y	N	—	—	—	N

(Continued on next page)

Table 1. Continued

Pt. No.	Exp. ID*	Sex	Age	Pathology (Grade)	Ini. KPS	Tx		MRI Finding		Experimental Data												
						Rad. Surg.	CCRT	Tumor Size	C/L	PFS (Wk)	OS (Wk)	Status	Subtype	Sphere Form. ^b	In Vivo Tumor Form. ^c	Invas. ^d	PCNA LI	MVD	Gene Exp.			
																				Rad. Surg.	CCRT	Inv.
55	I10-046	F	59	GBM (IV)	80	Y	Y	2.3 x 1.5	N	3	24.4	6	47	64	0	ND	Y	Y	N	67.1	15	N
56	I10-047	M	45	GBM (IV)	80	Y	Y	6.5 x 4.5	N	3	45.8	36	14	63	1	C	Y	Y	Y	76.3	46	Y
57	I11-067	F	46	GBM (IV)	70	Y	Y	1.2 x 0.8	N	3	15.5	ND	36	56	0	ND	Y	Y	N	45.1	36	N
58	I11-074	M	59	GBM (IV)	70	Y	Y	3.5 x 2.9	N	2	48.0	9	50	50	0	C	Y	Y	Y	41.8	23	Y
59	I11-100	M	25	GBM (IV)	80	Y	Y	7.0 x 5.3	N	1	22.1	11	39	39	0	ND	Y	Y	N	50.6	25	N

Abbreviations are as follows: C, classical; CCRT, concurrent chemoradiotherapy; C/L, contralateral; Form., formation; Gene Exp., gene expression profiling; Inv., involved; Invas., invasiveness; LI, labeling index (number of positive cells from randomly selected 100 cells); M, mesenchymal; MVD, microvessel density; N, neural; ND, not determined; OS, overall survival; P, proneural; PFS, progression free survival; status: 0 = alive, 1 = dead, 2 = follow-up loss; Rad. Surg., radical surgery; UD, undetermined; Wk, weeks. P00-000 = PC-NS00-000, I00-000 = IFCR-GBM00-000. See also Figure S1.

^aThe invasiveness of patients' tumors was defined as: 0 = no invasion, 1 = distance of invasion < 2 x diameter of tumor mass, 2 = 2 x diameter of tumor mass < distance of invasion < 3 x diameter of tumor mass, and 3 = 3 x diameter of tumor mass < distance of invasion.

^bWhen spheres (diameter ≥ 50 μm) were formed in the primary culture within 7 days, the GBM cells were reported to have in vitro sphere forming capacity.

^cIn vivo tumorigenicity was defined as tumor formation in the mouse brains within 12 months after tumor cell injection, which showed pathologic characteristics of the GBM.

^dThe invasiveness of orthotopic xenograft tumors was defined as Y = distance of infiltration > 2 x diameter of main mass in the paraffin sections.

distance of invasion with diameter of tumor (Table 1). Interestingly, comparison of the patient MRI and invasiveness of xenograft tumors revealed that invasiveness of parental and corresponding xenograft tumors were significantly correlated (n = 42, χ^2 test, p = 0.029).

- (2) Proliferation index (Figure 2B): proliferation index of xenograft tumors was positively correlated with that of their parental tumors (n = 53, Pearson correlation, p < 0.001).
- (3) Microvessel density (Figure 2C): CD31-positive microvessel density of xenograft tumors showed significant positive correlation with that of their parental tumors (n = 53, Pearson correlation, p < 0.001).

Genomic Similarity

To further examine the similarities between parental tumors and the corresponding orthotopic xenograft tumors, we performed genomic analysis. First, we performed short tandem repeat (STR) genotyping to ensure that each GBM xenograft was derived from the specific patient (Figure 3A). Analysis of array-comparative genomic hybridization (aCGH) (Figure 3B) and genetic mutation (Figure 3C) indicated that all examined genomic alterations found in the parental GBMs including copy number variations and genetic mutations were precisely replicated in the corresponding xenograft tumors.

A recent large genomic study categorized GBMs into four subgroups (proneural, neural, classical, and mesenchymal) (Cancer Genome Atlas Research Network, 2008; Phillips et al., 2006; Verhaak et al., 2010) based on their distinct gene expression signatures. In order to determine whether our library covers full spectrum of these subtypes and test whether gene expression signatures of a parental tumor are maintained in the orthotopic xenograft tumor, we performed global gene expression profiling analysis. We analyzed 58 GBM patients' surgical specimens, for which microarray gene expression data were available (Table 1). We also performed tissue microarray (TMA) analysis that encompasses the parental GBMs and corresponding orthotopic xenograft tumors. For the subtype determination, we adopted the nearest template prediction algorithm (Hoshida, 2010) for single-sample-based determination of subtypes. The analysis identified 18 proneural, 6 neural, 13 classical, and 19 mesenchymal GBMs in the data set (two undetermined; Table 1; Figure 3D). On TMA sections, we performed a series of immunohistochemical analysis against distinct GBM subtype markers; DLL3, SOX2, and Olig2 (proneural), MBP (neural), PDGFA and EGFR (proneural), CHI3L1, MAP2, and TOP2A (mesenchymal) (Phillips et al., 2006; Verhaak et al., 2010). Preferential expression of each subtype marker proteins was detected both in the parental GBM specimens and the corresponding xenograft tumors (Figure 3E).

Functional Relevance

We examined whether the patient-specific response to standard therapies could be replicated in the orthotopic xenograft tumor models.

Radiation Therapy

We arbitrarily chose five patients who had received radiation treatment in the clinic after resection of primary tumors (four

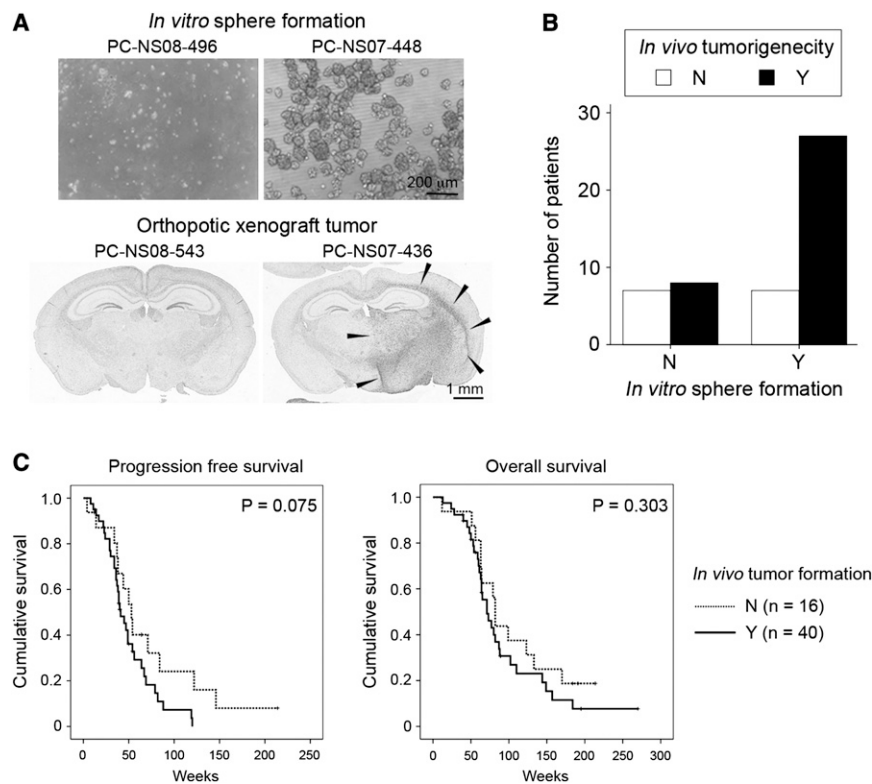


Figure 1. Primary Cultures and Orthotopic Xenograft Animal Models Derived from GBM Surgical Samples

(A) Acutely dissociated GBM cells were primarily cultured in the NBE condition or stereotactically injected into the brains of immune-compromised NOG mice. Immunohistochemistry against PCNA was illustrated for orthotopic xenograft tumors. Arrowheads indicate the border of a PCNA-positive xenograft tumor.

(B) Correlation between *in vitro* sphere formation capacity and *in vivo* tumorigenicity of acutely dissociated GBM cells was analyzed by the Fisher's exact test ($p = 0.09$).

(C) The PFS and OS of the GBMs with *in vivo* tumorigenic potential ($n = 40$) were compared with those without the potential ($n = 16$) by using the Kaplan-Meier plots and log rank test.

See also [Figure S2](#).

from our library, one from our recently published study ["827," PFS = 128 weeks] [Son et al., 2009]), and subjected their corresponding xenograft tumors to *in vivo* whole brain irradiation (2Gy daily for 5 days). Survival of the mice bearing PC-NS07-448, PC-NS07-464, PC-NS08-578, PC-NS09-780, and 827 tumors was differentially increased by the radiation therapy ($21.9\% \pm 7.1\%$, $49.8\% \pm 14.1\%$, $45.9\% \pm 8.6\%$, $23.3\% \pm 19.5\%$, and $45.0\% \pm 5.9\%$, respectively, [Figures 4A](#) and [S4A](#)). The increment of survival was positively correlated with the PFS of the parental tumors ([Figure 4A](#)). Radiation-mediated survival benefits of the mice bearing the GBMs (PC-NS07-448 and PC-NS09-780) whose parental tumors have relatively short-PFS, are significantly less than those of the other GBMs with longer PFS ([Figure 4A](#)), suggesting that the radiation-response of the parental GBM can be predicted by the xenograft tumor model.

To further elucidate clinical implications of the differential response to the radiation therapy, we derived Radio-Response (RR) signature by comparing gene expression alteration of the radioresistant PC-NS07-448 ("448") and radiosensitive PC-NS07-464 ("464") xenograft tumors after the radiation therapy ([Figure S4B](#); [Tables S1](#) and [S2](#); [Extended Experimental Procedures](#)). Based on the gene expression, high-grade gliomas in the REMBRANDT data set ($n = 463$) (Madhavan et al., 2009) were clustered into 448-like ($n = 267$) and 464-like ($n = 196$) group ([Figure S4B](#)). When we restrict the samples to 219 GBMs (grade IV), 174 and 45 GBMs were clustered into 448-like and 464-like group, respectively. Both the 448-like high-grade gliomas and GBMs showed significantly worse clinical outcome than the

464-like groups ([Figure S4B](#)), confirming the clinical relevance of the RR signature.

Chemotherapy

GBM patients differentially respond to the TMZ-based chemotherapy depending on the methylation status of the *MGMT* gene promoter (Hegi et al., 2005; Stupp et al., 2005). We tested whether the differential response could be reproduced in xenograft tumors. In agreement with the clinical observation, TMZ chemotherapy prolonged the OS of mice with *MGMT*-methylated PC-NS07-464 tumors ($148.5\% \pm 45.4\%$) significantly more than that of mice harboring *MGMT*-unmethylated PC-NS09-559 tumors ($55.7\% \pm 38.6\%$, $p < 0.001$, [Figure 4B](#)).

Targeted Therapy

The hypervascular nature of GBMs has suggested that antiangiogenic treatment, such as the VEGF-neutralizing antibody, bevacizumab, may have beneficial activity. Although it showed treatment effects on the animal model using a conventional GBM cell line, U-87MG (de Groot et al., 2010), it failed to elongate OS of GBM patients compared to that of standard treatment controls (Lai et al., 2011). When we tested anti-tumor activity of bevacizumab, survival of mice with PC-NS07-448, PC-NS07-464, PC-NS08-559, or PC-NS09-748 xenograft tumors was not altered by bevacizumab treatment ([Figure 4C](#)). Although OS was not altered, the treatment made xenograft tumors more invasive ([Figure 4C](#)). These morphological changes were also observed in human GBMs with bevacizumab treatment (Lai et al., 2011), which suggest that xenograft tumors derived from GBM surgical samples would predict the results of clinical trial.

Genetic Signature of *In Vivo* Tumorigenic Potential

Our data indicated that *in vivo* tumorigenic potential of primarily cultured GBM cells is associated with clinical aggressiveness of the corresponding patients, although it was not statistically significant ([Figure 1C](#)). We reasoned that the shortage of statistical significance was due to the small sample size, and that the

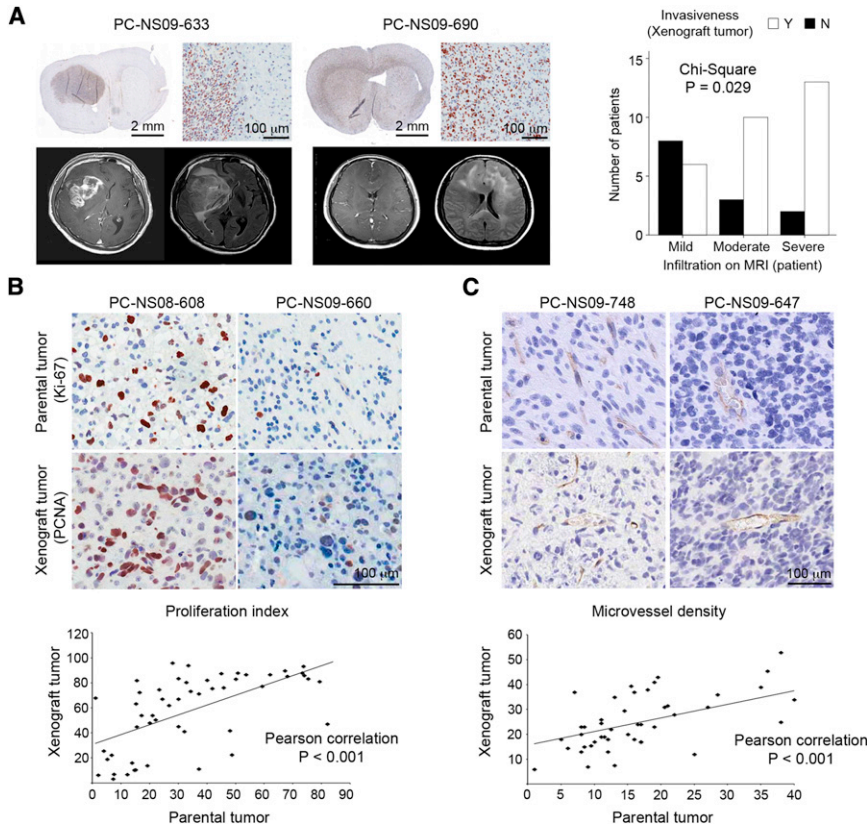


Figure 2. Representation of Morphologic and Pathologic Characteristics of Parental GBMs by the Corresponding Orthotopic Xenograft Tumors

(A–C) The invasiveness (A), proliferation index (B), and microvessel density (C) of the parental and corresponding orthotopic xenograft tumors were analyzed and compared. (A) The invasive parental and xenograft tumor was defined by comparisons of the distances of infiltration with the diameters of main mass in MRI and pathologic sections, respectively. (B) Proliferation index was analyzed by immunohistochemistry against Ki-67 (parental GBMs) or PCNA (xenograft GBMs) and then calculated as number of positive cells from 100 cells selected randomly. Each index was analyzed three times and the average was utilized for the statistical analysis. (C) Microvessel density was analyzed by immunohistochemistry against CD31. Three microscopic fields were randomly selected at 200 \times magnification and the numbers of CD31-positive microvessels were calculated. Averages for the three were utilized for the statistical analysis.

See also [Figure S3](#).

The analysis revealed that pathways related to cell cycle, telomere maintenance, transcription, Notch signaling, or Wnt signaling were upregulated in the GBMs with in vivo tumorigenic potential, whereas pathways related to neuronal

gene expression difference between the tumorigenic and nontumorigenic groups may nonetheless capture information that is useful for predicting patient survival and understanding biological underpinnings of differential aggressiveness. We therefore defined the “tumorigenesis” signature composed of 709 differentially expressed genes (change more than 1.5-fold; [Figure 5A](#); [Table S3](#)) between tumorigenic ($n = 36$; [Table 1](#); [Figures S1A](#) and [S1C](#)) and nontumorigenic GBMs ($n = 10$). To validate this signature, we applied this to two independent GBM gene expression profiling data sets, the Cancer Genome Atlas (TCGA) ([Cancer Genome Atlas Research Network, 2008](#); [Verhaak et al., 2010](#)) and REMBRANDT ([Madhavan et al., 2009](#)). Nearest template prediction algorithm allowed for prediction of each GBM patient into two groups, each either positively or negatively associated with the tumorigenesis signature. When patient survival was compared between the two groups, the positive-group showed significantly worse survival than the negative-group with the REMBRANDT data set ($p < 0.0001$, log rank test; [Figure 5B](#)). Permutation analysis indicated that such or more severe separation in survival is unlikely observed by chance ($p = 0.004$), potentiating the validity of the signature ([Figure S5A](#)). The statistically significant trend was also observed with the TCGA data set ($p = 0.019$, log rank test, data not shown).

To investigate the biological underpinnings of the differential tumorigenic potential and the clinical aggressiveness, we turned to pathway analysis using the gene set enrichment analysis (GSEA) ([Clark and Ma’ayan, 2011](#); [Subramanian et al., 2005](#)).

or immune functions were downregulated ([Table S4](#)). If these pathways influence clinical aggressiveness in GBMs, the activity of the pathways would predict patient survival. We devised a method to calculate pathway activity for each patient based on the gene expression profile; the pathway activity is defined between -1 and 1 , with the score bigger than 0 and smaller than 0 indicating up- and downregulation, respectively. When the pathway activity for the PITX2 pathway (PITX2 is a transcription factor, acting downstream of WNT) was calculated for each patient of the REMBRANDT data set, we detected that the ones upregulating the pathway corresponds to the ones with poorer survival ($p = 0.002$, log rank test; [Figure 5C](#)). Alternatively, by Cox proportional hazard regression, high pathway activity was significantly correlated with poor patient survival ($p = 0.007$, one-sided Wald test; [Figure 5D](#)). When this analysis was expanded to five most highly upregulated and downregulated pathways in the BIOCARTE ([Figure 5D](#)), KEGG ([Figure S5B](#)), and REACTOME ([Figure S5C](#)) databases, we observed the significant trend that the pathways upregulated or downregulated in the GBMs with in vivo tumorigenic potential are correlated with poor or favorable patient survival, respectively ($p < 0.05$ for all three databases, KS test).

As the GBMs that made invasive tumors ($n = 29$) in the mouse brain showed significantly worse clinical outcomes in our data set, when compared to those that made noninvasive (demarcated) tumors ($n = 13$) or did not made tumors ($n = 16$) ([Figure S2B](#)), we sought for the opportunity to further stratify

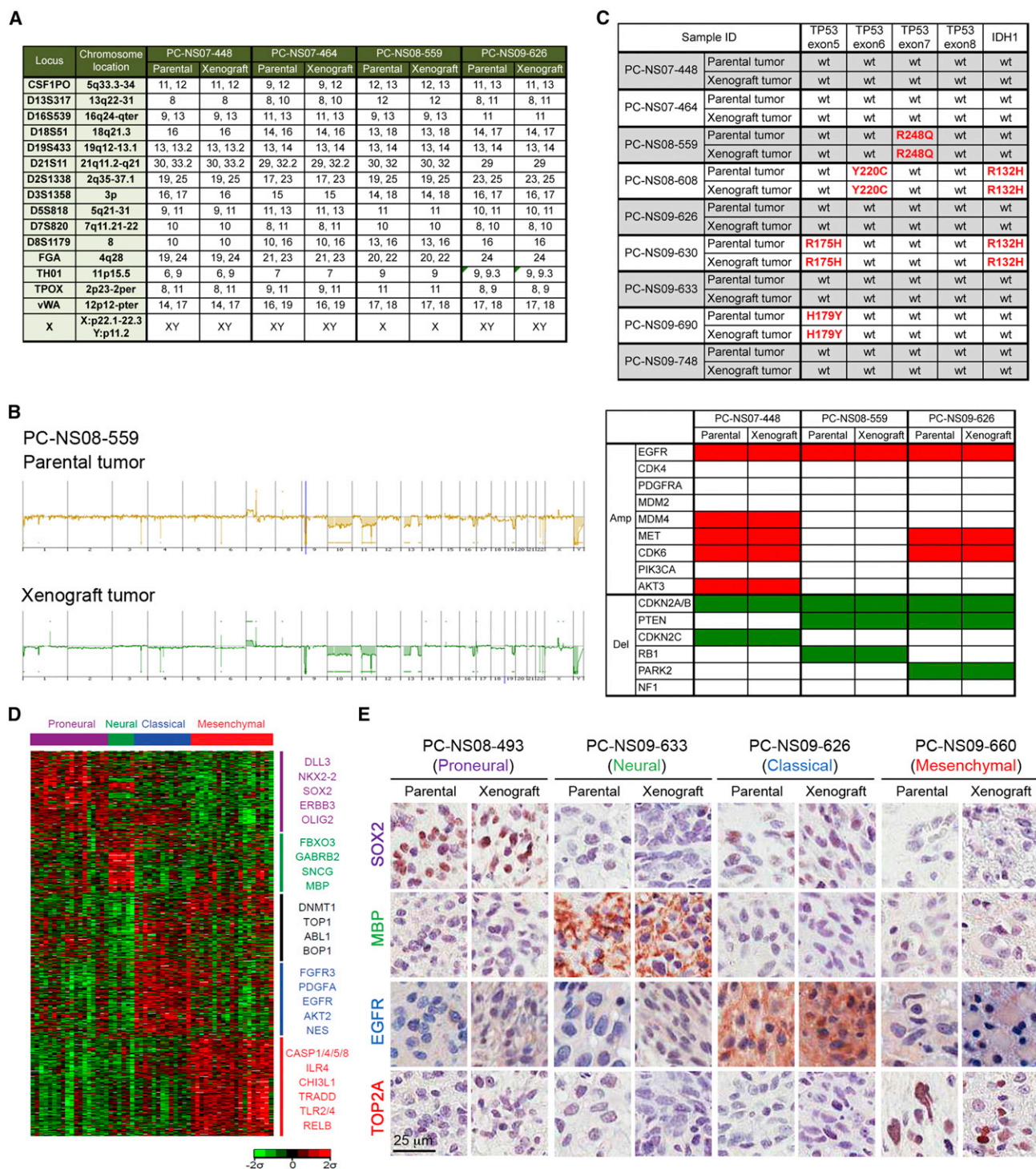


Figure 3. Molecular Characteristics of Parental and Orthotopic Xenograft Tumors

(A–E) Short tandem repeat (A), genomic copy number variation (B), genetic mutation of *TP53* and *IDH1* (C), and gene expression pattern (D and E) of parental GBMs were compared with those of the corresponding orthotopic xenograft tumors. (B) Genomic copy number variation was analyzed by aCGH (left), and the genomic copy number variations of the genes that were reported to be altered frequently in GBMs were summarized (right; red, amplified; green, deleted). (C) Specific mutations were indicated by red. wt, wild-type. (D) Subtypes of the 58 GBM samples were determined by the Nearest Template Prediction method. (E) Expression of gene products was compared immunohistochemically between parental GBMs and orthotopic xenograft tumors using TMA containing 11 parental GBMs and corresponding orthotopic xenograft tumors. Nuclei are presented in blue. See also Table S6.

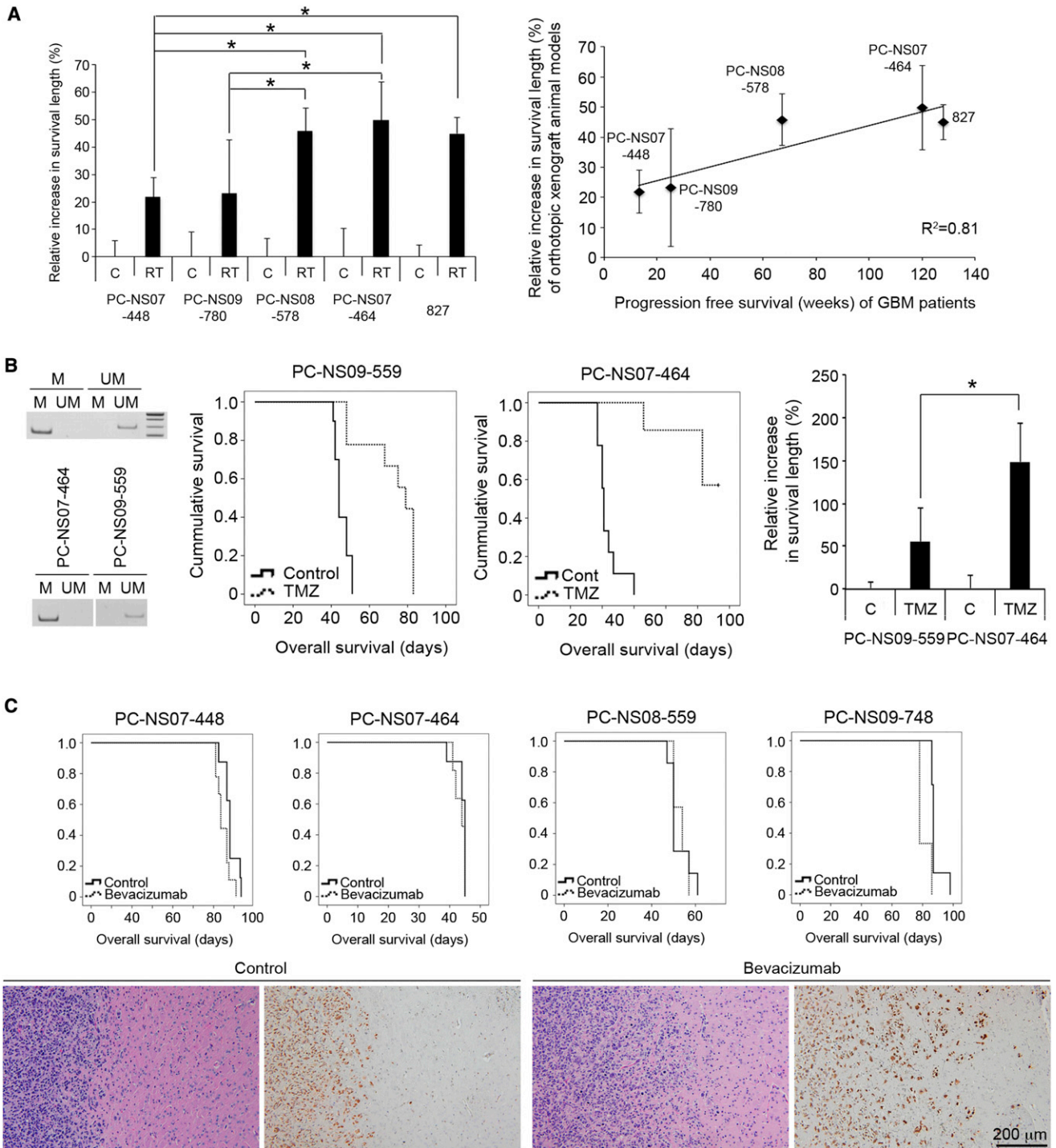


Figure 4. Functional Representation of Treatment Responsiveness of Parental Tumors by the Corresponding Orthotopic Xenograft Tumors
 (A) Xenograft tumors derived from PC-NS07-448, PC-NS07-464, PC-NS08-578, PC-NS09-780, or 827 tumor (n = 8, 15, 9, 9, and 4 for the control [C] group, n = 9, 9, 10, 9, and 4 for the radiation [RT] group, respectively) were treated with whole brain radiation therapy (2Gy daily for 5 days since 50% median survival time passed). OS was calculated and then increase in the survival length by the whole brain irradiation was compared (left). *p < 0.05. Increase in the survival length of xenograft tumors was correlated with PFS of parental tumors (right). Error bar represents SD.
 (B) Methylation status of the *MGMT* promoter was analyzed by methylation specific PCR (left, M, methylation specific primers or methylated control gDNA; UM, methylation specific primers or unmethylated control gDNA). Xenograft tumors derived from PC-NS07-464 or PC-NS09-559 (n = 9, 10 for the control [C] group, n = 7, 9 for the TMZ group, respectively) were treated with TMZ (65 mg/kg, oral administration, daily since 50% median survival time passed). OS was calculated and then increase in the survival length by the TMZ chemotherapy was compared. *p < 0.05. Error bar represents SD.

(legend continued on next page)

tumorigenic GBMs based on their differential invasiveness. To validate whether the group with the invasion property represents more aggressive GBMs, we compared gene expression of the “invasive” ($n = 29$) and “demarcated” ($n = 13$) groups. We identified 777 differentially expressed genes (change more than 1.5-fold; Figure S6A; Table S5; Extended Experimental Procedures), which was defined as the “invasion” signature. To validate this signature, we again used the REMBRANDT data sets, as did for the tumorigenesis signature. When patient survival time was compared between the two groups, the invasive group showed significantly worse survival than the demarcated group ($p = 0.027$, log rank test; Figure S6B), suggesting possible clinical relevance of the invasion signature.

DISCUSSION

There have been many efforts and interests on the xenograft tumors derived from the patient cancer cells as human cancer surrogates for therapeutic purposes (DeRose et al., 2011; Fu et al., 1992; Giannini et al., 2005; Groves et al., 2002; Horten et al., 1981; Karam et al., 2011; Marangoni et al., 2007; Rubio-Viqueira et al., 2006; Wang et al., 2009; Xie et al., 2008; Yi et al., 2011; Zhuo et al., 2010). However, the concept, “preclinical animal models derived from primary cancer cells would recapitulate their parental tumors faithfully,” remains unsolved because the molecular and biological validity of preclinical models has not been rigorously tested by a large-scale library. The results presented in this manuscript may provide an in-depth validation to support the above concept.

Tumor microenvironment can critically affect the biological behavior of xenograft tumors (Charles et al., 2011; Langley and Fidler, 2011; Lathia et al., 2011). Infiltrative pattern of GBM growth, a critical pathological characteristic of human GBM, was frequently lost when the tumor graft was established in mice flanks (Antunes et al., 2000). Therefore, orthotopic implantation of our study would overcome potential limitations associated with heterotypic transplantation in the previous studies (DeRose et al., 2011; Fu et al., 1992; Giannini et al., 2005; Groves et al., 2002; Horten et al., 1981; Karam et al., 2011; Marangoni et al., 2007; Rubio-Viqueira et al., 2006; Wang et al., 2009; Yi et al., 2011; Zhuo et al., 2010) and increase the validity of the preclinical platform. Our xenograft model still has caveats, as the murine brain microenvironment has molecular and functional differences in comparison to the human brain microenvironment. Future development of mouse models such as reducing the incompatibility of cytokines and integrins between species would help better mimic the natural tumor environment of human GBM.

Differential clinical response of GBMs to TMZ chemotherapy according to the MGMT expression (Hegi et al., 2005; Stupp et al., 2005) and accumulating evidence indicating GBM

heterogeneity in the genomic make-ups and phenotypic properties (Martens et al., 2008; Sausville and Burger, 2006; Taillandier et al., 2003) potentiate personalized approach for the maximal therapeutic benefit. This study could present conceptual and experimental background for the personalized translational research with functional genomics. Our data support the following notion: (1) orthotopic xenograft animal models could predict differential results of clinical treatment of the parental tumors, (2) the translational platforms we built represent intratumoral heterogeneity of human GBMs to therapeutic modalities, and (3) analysis of genetic differences between responding and nonresponding xenograft tumors could draw clinically meaningful biomarkers discriminating patient populations with different prognosis. Based on these capacities, the personalized preclinical/translational research would lead to more successful rationale-driven clinical trials with target subpopulation for newly developed therapeutic agents. Although this article was focused to GBMs, these translational implications would be adoptable to other cancer types.

Significant association between the capacity of forming a xenograft tumor and clinical aggressiveness of the parental GBMs has several important preclinical and clinical implications. First, bidirectional approaches between translational library and cancer patient population. A preclinical platform could represent the specific responses of cancer patients to a newly developed anticancer agent. Conversely, novel therapeutic and/or diagnostic targets for cancer patients could be identified by analysis of preclinical models. In this study, we successfully identified the molecular candidates to discriminate GBM patients with worse clinical prognosis using *in vivo* tumorigenicity of primary GBM cells or invasive properties of resulting xenograft tumors, and validated them using independent GBM data sets. Second, translational models representing aggressive pheno- and genotypes of the GBM would provide ideal preclinical models for the rationale-driven clinical trials overcoming the treatment resistance of the GBM, because aggressive pheno- and genotypes of the GBM would be manifested by the treatment resistance.

In summary, we demonstrated that orthotopic GBM xenograft models derived from the acutely dissociated GBM cells are preclinically and clinically relevant models that can functionally represent the biology of human GBMs *in situ*.

EXPERIMENTAL PROCEDURES

GBM Patients and Primary Cell Culture

Following informed consent, surgical specimens and clinical records were obtained from 59 GBM patients who had brain tumor removal surgery at the Samsung Medical Center (Seoul, Korea) in accordance with the appropriate Institutional Review Boards (Table 1). Tumors were classified as GBM based on WHO criteria by examination of pathologists (Louis et al., 2007).

(C) Xenograft tumors derived from PC-NS07-448, PC-NS07-464, PC-NS09-559, or PC-NS09-748 ($n = 8, 8, 7,$ and 7 for the control group, $n = 9, 11, 7,$ and 6 for the Bevacizumab group, respectively) were treated with Bevacizumab (10 mg/kg, intraperitoneal injection, twice per week since 50% median survival time passed). Morphologic alteration of the xenograft tumors by Bevacizumab treatment was analyzed by H&E and immunohistochemistry against human nuclei (low, PC-NS07-464).

See also Tables S1, S2, and Figure S4.

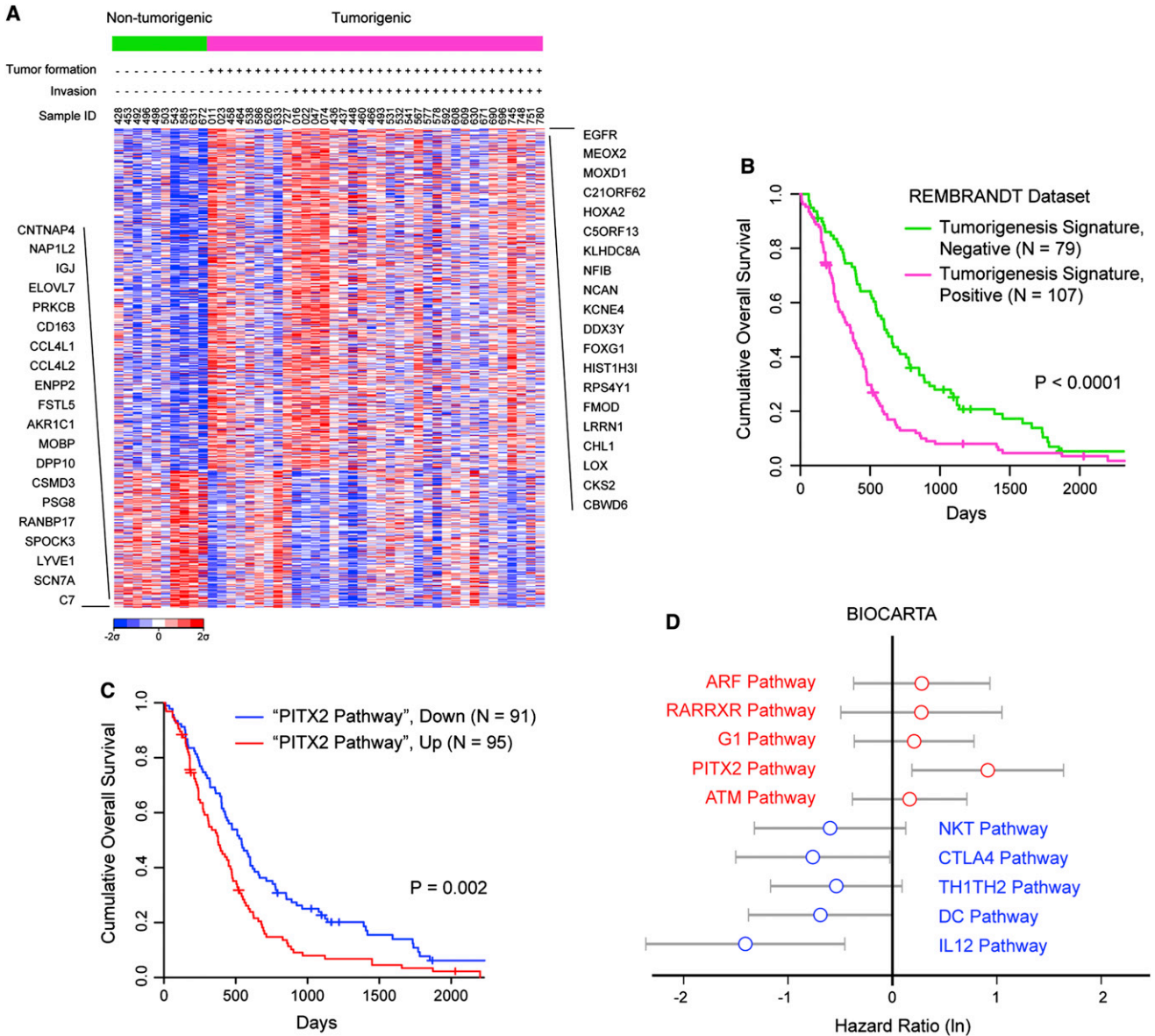


Figure 5. The Tumorigenesis Signature, Tumorigenesis-Associated Pathways, and Their Association with Clinical Outcome in an Independent Data Set

(A) Expression of 709 genes that are differentially expressed (cutoff, change more than 1.5-fold) between 10 nontumorigenic and 36 tumorigenic GBMs, plotted as a heat map after row-normalization. Red and blue indicate high and low expression, respectively. The 20 genes most highly differentially expressed with each group are listed on the sides.

(B) A Kaplan-Meier plot comparing cumulative OS of two groups of patients in the REMBRANDT data set, with each group either positively or negatively associated with the tumorigenesis signature.

(C) A Kaplan-Meier plot comparing the OS of two groups of patients in the REMBRANDT data set, with each group either up- or downregulating the PITX2 pathway ($p = 0.002$, log rank test).

(D) A forest plot displaying hazard ratios (in a natural log scale) and their 95% confidence intervals, with each hazard ratio representing the correlation between the calculated activity of a given pathway and the OS of patients in the REMBRANDT data set. The top five (red) and bottom five (blue) entries correspond to the pathways in BIOCARTA that were found most up- and downregulated, respectively, in the group positively associated with the tumorigenesis signature.

See also Table S3, S4, and S5, and Figures S5 and S6.

Parts of the surgical samples were enzymatically dissociated into single cells, following the procedures previously reported (Joo et al., 2008). Dissociated GBM cells were cultured in neurobasal media with N2 and B27 supplements (0.5x each; Invitrogen) and human recombinant bFGF and EGF (25 ng/ml

each; R&D Systems) (NBE condition). Alternatively, acutely dissociated GBM cells in the NBE condition were plated on the flasks, coated with Laminin (Sigma) overnight at 10 μ g/ml prior to use, for the adherent culture (Pollard et al., 2009).

Orthotopic Xenograft Animal Model

Animal experiments were approved by the Institutional Review Boards of the Samsung Medical Center and conducted in accordance with the "National Institutes of Health Guide for the Care and Use of Laboratory Animals" (NIH publication 80-23). Acutely dissociated GBM cells were stereotactically (2 mm left and 1 mm anterior to the bregma, 2 mm deep from the dura) injected into the brains of NOG mice (Ito et al., 2002) within 12 hr after surgery (2.5×10^4 – 1.0×10^5 cells in 10 μ l HBSS for each mice, $n = 4$ –9 for each sample). Mice with the reduction of the total body weight (>20%) were sacrificed, and brains were processed for paraffin or frozen section.

Whole-Brain In Vivo Irradiation, TMZ Chemotherapy, and Bevacizumab-Targeted Therapy

Orthotopic xenograft tumors were made as described previously, using primarily cultured GBM cells that had short term in vitro culture in the NBE condition (in vitro passage <6, 2.0×10^5 cells for each animal). Treatments were started at the half of the median survival length of the orthotopic xenograft animal models. The reduction of the total body weight (>20%) was regarded as mortality. Whole brain 2Gy X-irradiations were applied daily for 5 days (total 10Gy) using a blood irradiator (IBL-437C, CIS-US). Mouse bodies were shielded with a custom-made lead shield device. TMZ (65 mg/kg) was orally administrated daily. Methylation status of the MGMT gene promoter was determined as previously reported (Yang et al., 2009). Bevacizumab (10 mg/kg, twice per week) was injected into the intraperitoneal space.

TMA and Immunohistochemistry

A TMA containing 11 parental GBMs and corresponding orthotopic xenograft tumors (PC-NS07-464, PC-NS08-493, PC-NS08-532, PC-NS08-559, PC-NS08-608, PC-NS09-626, PC-NS09-630, PC-NS09-633, PC-NS09-660, PC-NS09-690, and PC-NS09-696) was produced as previously described (Kong et al., 2009). Immunohistochemistry was performed as described previously (Kong et al., 2009). Primary antibodies included Ki-67, PCNA (DAKO), DLL3 (Santa Cruz), SOX2, Olig2, MAP2 (Abcam), MBP, PDGFA, EGFR (Santa Cruz), CHI3L1, TOP2A (LifeSpan Bioscience), and CD31 (DAKO for xenograft tumors and BD Pharmingen for parental tumors).

STR Genotyping, aCGH, and Genetic Mutation of TP53 and IDH1

Genomic DNA was isolated from tumor sample using QIAamp DNA mini kit (QIAGEN). For STR genotyping, target DNA was amplified by multiplex PCR for 16 loci using the AmpFISTR Identifier PCR Amplification Kit (Applied Biosystems). PCR products mixed with internal size standard (GS-500 LIZ, Applied Biosystems) were electrophoresed in an ABI 3130xl Genetic Analyzer (Applied Biosystems) and analyzed with GeneMapper 4.0 software using the supplied allelic ladders (Applied Biosystems). aCGH was performed using the Agilent Human Whole Genome CGH 244K microarray. For genetic mutation of *TP53* and *IDH1*, PCR reactions (40 cycles, at 95°C for 30 s, 58°C for 30 s, and 72°C for 30 s) were carried out in 20 μ l volume that contained 100 ng of gDNA, 200 nM each primer (Table S6), and Maxime PCR premix (iNtRON). PCR products were purified by QIAquick PCR purification kit (QIAGEN) and bidirectional sequencing was performed using the BigDye Terminator v1.1 kit (Applied Biosystems) on an ABI 3130xl genetic analyzer (Applied Biosystems).

Gene Expression Profiling

Gene expression profiling was conducted using Affymetrix Human Gene 1.0 ST arrays. The resulting CEL files were normalized using Robust Multichip Averaging procedure. PM-MM difference model was used to obtain the expression values. The probe IDs were resolved into gene names by using GSEA-P program (downloadable from Broad Institute website). For the REMBRANDT data set (Madhavan et al., 2009), CEL files for high-grade glioma samples were downloaded from the website (<https://caintegrator.nci.nih.gov/rembrandt/>), along with a matching clinical information file. The CEL files were processed as were the in-house produced CEL files, except a matching array annotation file (for Affymetrix U133 Plus 2.0 array) was used. For the TCGA data set (Cancer Genome Atlas Research Network, 2008; Verhaak et al., 2010), gene expression data files for 556 GBM samples

originally produced using Affymetrix U133A 2.0 arrays were downloaded from the official website, along with a matching clinical information file. The gene expression files were provided in an already processed form (Level III).

GBM Subtype Prediction

Among the 840 marker genes originally used to classify GBM subtypes (Verhaak et al., 2010), 787 were represented in the microarray platform we used. The 787 genes were annotated with the numeric code representing the unique subtype that each gene represents (1, 2, 3, and 4 for proneural, neural, classical, and mesenchymal markers, respectively, and 5 for the rest). The marker gene information file and the file containing the gene expression data for 58 GBM samples were loaded into Nearest Template Prediction module in GenePattern (available through Broad Institute). All samples were classified into one of the five categories with statistical significance (with Bonferroni p value below 0.05, bootstrap test with 1,000 resampling).

Gene Signature Analysis

The 46 in-house-profiled GBM samples were subject to the tumorigenesis signature analysis (Figures S1A and S1C). Genes differentially expressed (changes more than 1.5-fold) between the tumorigenic and nontumorigenic group ($n = 36$ and 10, respectively) were identified. The tumorigenesis signature was composed of the differentially expressed genes, with each labeled with the associated subgroup and a value for log₂-fold change. The signature was loaded into the Nearest Template Prediction module in GenePattern. Also loaded into the module was either the REMBRANDT or the TCGA data set in GCT format. The module produced an output file with classification of samples in each data set. Survival analysis (Kaplan-Meier plot and log rank test) was performed using R Survival package. For permutation analysis, we randomly regrouped the GBM patients into tumorigenesis and nontumorigenesis subgroups, maintaining the size of the original subgroups. A "control" signature was derived and applied to the REMBRANDT data set for prognostic prediction, as was done with the original unshuffled data set. The fraction of the resulting 500 p values (from log rank test) smaller than the original p value of the unshuffled data set ($p = 0.000046$) was defined as the p value of the permutation test.

Pathway Analysis

Identification of the In Vivo Tumorigenesis-Associated Pathways

The 46 in-house-profiled GBM samples were subject to pathway analysis by using the GSEA-P program. The analysis utilized gene sets in MSigDB v3.0: specifically gene sets that are derived from three major manually-curated pathway databases: KEGG, REACTOME, and BIOCARTA. Genes were ranked and weighted by the degree of differential expression, quantified by Z scores (adjusted from T scores of t test). For the permutation_type parameter: an alternative option (gene_set) was used instead of the default option (phenotype). This alternative setting tends to give more generous p values; indeed, many of the in vivo tumorigenesis-associated pathways listed in Table S4 fell below a traditional significance cutoff (FDR < 0.25) under the default setting. We nonetheless used the alternative setting, because (1) the default setting is likely to give excessively conservative significance assessments when the number of samples is small, and (2) most of the pathways that pass the significance cutoff only at the alternative setting showed the expected trend of correlation with patient survival in the REMBRANDT data set.

Quantification of Pathway Activity from a Gene Expression Data Set

For the REMBRANDT data set, expression values were "gene-normalized": for each gene, the log expression value for each sample was offset by the average log expression value of the gene across all the samples. To calculate the activity of a given pathway in a given sample, the relative expression values of the pathway genes were compared to the relative expression values of all genes. KS score (Python Stats package) was used for the comparison; the score is defined between -1 and 1, with the value bigger and smaller than 0 indicates the pathway genes are up- and downregulated, respectively, compared to all genes in the given sample. R Survival package was used to (1) plot patient survival of samples up- and downregulating a given pathway, (2) assess statistical significance of the difference in survival between the

two groups, and (3) calculate hazard ratio of the KS score (pathway activity) for OS (by the Cox proportional hazard regression).

ACCESSION NUMBERS

The GEO accession number for the gene expression and CGH data reported in this article is GSE42670.

SUPPLEMENTAL INFORMATION

Supplemental Information includes Extended Experimental Procedures, six figures, and six tables and can be found with this article online at <http://dx.doi.org/10.1016/j.celrep.2012.12.013>.

LICENSING INFORMATION

This is an open-access article distributed under the terms of the Creative Commons Attribution-NonCommercial-No Derivative Works License, which permits non-commercial use, distribution, and reproduction in any medium, provided the original author and source are credited.

ACKNOWLEDGMENTS

This study was supported by a grant of the Korea Healthcare technology R&D project, Ministry for Health & Welfare Affairs, Republic of Korea (A092255), and by a Global Frontier Project grant (NRF-2012M3A6A-2010-0029781, 0029785) and the WCU project (R3-2008-000-10103-0) of the National Research Foundation funded by the Ministry of Education, Science and Technology of Korea. We thank Soonmyung Paik (Samsung Cancer Research Institute) for valuable scientific suggestions and Stephanie Sunny Ahn for help with illustrations. As a scientific resource for GBM, our GBM models would be distributed upon requests.

Received: January 17, 2012

Revised: August 20, 2012

Accepted: December 20, 2012

Published: January 17, 2013

REFERENCES

Adamson, C., Kanu, O.O., Mehta, A.I., Di, C., Lin, N., Mattox, A.K., and Bigner, D.D. (2009). Glioblastoma multiforme: a review of where we have been and where we are going. *Expert Opin. Investig. Drugs* 18, 1061–1083.

Antunes, L., Angioi-Duprez, K.S., Bracard, S.R., Klein-Monhoven, N.A., Le Faou, A.E., Duprez, A.M., and Plénat, F.M. (2000). Analysis of tissue chimerism in nude mouse brain and abdominal xenograft models of human glioblastoma multiforme: what does it tell us about the models and about glioblastoma biology and therapy? *J. Histochem. Cytochem.* 48, 847–858.

Bonavia, R., Inda, M.M., Cavenee, W.K., and Furnari, F.B. (2011). Heterogeneity maintenance in glioblastoma: a social network. *Cancer Res.* 71, 4055–4060.

Cancer Genome Atlas Research Network. (2008). Comprehensive genomic characterization defines human glioblastoma genes and core pathways. *Nature* 455, 1061–1068.

Charles, N.A., Holland, E.C., Gilbertson, R., Glass, R., and Kettenmann, H. (2011). The brain tumor microenvironment. *Glia* 59, 1169–1180.

Chi, A.S., and Wen, P.Y. (2007). Inhibiting kinases in malignant gliomas. *Expert Opin. Ther. Targets* 11, 473–496.

Clark, N.R., and Ma'ayan, A. (2011). Introduction to statistical methods for analyzing large data sets: gene-set enrichment analysis. *Sci. Signal.* 4, tr4.

de Groot, J.F., Fuller, G., Kumar, A.J., Piao, Y., Eterovic, K., Ji, Y., and Conrad, C.A. (2010). Tumor invasion after treatment of glioblastoma with bevacizumab: radiographic and pathologic correlation in humans and mice. *Neuro. Oncol.* 12, 233–242.

DeRose, Y.S., Wang, G., Lin, Y.C., Bernard, P.S., Buys, S.S., Ebbert, M.T., Factor, R., Matsen, C., Milash, B.A., Nelson, E., et al. (2011). Tumor grafts derived from women with breast cancer authentically reflect tumor pathology, growth, metastasis and disease outcomes. *Nat. Med.* 17, 1514–1520.

Fu, X., Guadagni, F., and Hoffman, R.M. (1992). A metastatic nude-mouse model of human pancreatic cancer constructed orthotopically with histologically intact patient specimens. *Proc. Natl. Acad. Sci. USA* 89, 5645–5649.

Furnari, F.B., Fenton, T., Bachoo, R.M., Mukasa, A., Stommel, J.M., Stegh, A., Hahn, W.C., Ligon, K.L., Louis, D.N., Brennan, C., et al. (2007). Malignant astrocytic glioma: genetics, biology, and paths to treatment. *Genes Dev.* 21, 2683–2710.

Giannini, C., Sarkaria, J.N., Saito, A., Uhm, J.H., Galanis, E., Carlson, B.L., Schroeder, M.A., and James, C.D. (2005). Patient tumor EGFR and PDGFRA gene amplifications retained in an invasive intracranial xenograft model of glioblastoma multiforme. *Neuro. Oncol.* 7, 164–176.

Groves, M.D., Puduvalli, V.K., Hess, K.R., Jaecle, K.A., Peterson, P., Yung, W.K., and Levin, V.A. (2002). Phase II trial of temozolomide plus the matrix metalloproteinase inhibitor, marimastat, in recurrent and progressive glioblastoma multiforme. *J. Clin. Oncol.* 20, 1383–1388.

Hegi, M.E., Diserens, A.C., Gorlia, T., Hamou, M.F., de Tribolet, N., Weller, M., Kros, J.M., Hainfellner, J.A., Mason, W., Mariani, L., et al. (2005). MGMT gene silencing and benefit from temozolomide in glioblastoma. *N. Engl. J. Med.* 352, 997–1003.

Horten, B.C., Basler, G.A., and Shapiro, W.R. (1981). Xenograft of human malignant glial tumors into brains of nude mice. A histopathological study. *J. Neuropathol. Exp. Neurol.* 40, 493–511.

Hoshida, Y. (2010). Nearest template prediction: a single-sample-based flexible class prediction with confidence assessment. *PLoS ONE* 5, e15543.

Ito, M., Hiramatsu, H., Kobayashi, K., Suzue, K., Kawahata, M., Hioki, K., Ueyama, Y., Koyanagi, Y., Sugamura, K., Tsuji, K., et al. (2002). NOD/SCID/gamma(c)(null) mouse: an excellent recipient mouse model for engraftment of human cells. *Blood* 100, 3175–3182.

Joo, K.M., Kim, S.Y., Jin, X., Song, S.Y., Kong, D.S., Lee, J.I., Jeon, J.W., Kim, M.H., Kang, B.G., Jung, Y., et al. (2008). Clinical and biological implications of CD133-positive and CD133-negative cells in glioblastomas. *Lab. Invest.* 88, 808–815.

Karam, J.A., Zhang, X.Y., Tamboli, P., Margulis, V., Wang, H., Abel, E.J., Culp, S.H., and Wood, C.G. (2011). Development and characterization of clinically relevant tumor models from patients with renal cell carcinoma. *Eur. Urol.* 59, 619–628.

Kong, D.S., Song, S.Y., Kim, D.H., Joo, K.M., Yoo, J.S., Koh, J.S., Dong, S.M., Suh, Y.L., Lee, J.I., Park, K., et al. (2009). Prognostic significance of c-Met expression in glioblastomas. *Cancer* 115, 140–148.

Lai, A., Tran, A., Nghiemphu, P.L., Pope, W.B., Solis, O.E., Selch, M., Filka, E., Yong, W.H., Mischel, P.S., Liau, L.M., et al. (2011). Phase II study of bevacizumab plus temozolomide during and after radiation therapy for patients with newly diagnosed glioblastoma multiforme. *J. Clin. Oncol.* 29, 142–148.

Langley, R.R., and Fidler, I.J. (2011). The seed and soil hypothesis revisited—the role of tumor-stroma interactions in metastasis to different organs. *Int. J. Cancer* 128, 2527–2535.

Lathia, J.D., Heddleston, J.M., Venere, M., and Rich, J.N. (2011). Deadly teamwork: neural cancer stem cells and the tumor microenvironment. *Cell Stem Cell* 8, 482–485.

Lee, J., Kotliarova, S., Kotliarov, Y., Li, A., Su, Q., Donin, N.M., Pastorino, S., Purow, B.W., Christopher, N., Zhang, W., et al. (2006). Tumor stem cells derived from glioblastomas cultured in bFGF and EGF more closely mirror the phenotype and genotype of primary tumors than do serum-cultured cell lines. *Cancer Cell* 9, 391–403.

Louis, D.N., Ohgaki, H., Wiestler, O.D., Cavenee, W.K., Burger, P.C., Jouvet, A., Scheithauer, B.W., and Kleihues, P. (2007). The 2007 WHO classification of tumours of the central nervous system. *Acta Neuropathol.* 114, 97–109.

- Lutz, K., Radbruch, A., Wiestler, B., Bäumer, P., Wick, W., and Bendszus, M. (2011). Neuro-radiological response criteria for high-grade gliomas. *Clin Neuro-radiol* 21, 199–205.
- Madhavan, S., Zenklusen, J.C., Kotliarov, Y., Sahni, H., Fine, H.A., and Buetow, K. (2009). REMBRANDT: helping personalized medicine become a reality through integrative translational research. *Mol. Cancer Res.* 7, 157–167.
- Marangoni, E., Vincent-Salomon, A., Auger, N., Degeorges, A., Assayag, F., de Cremoux, P., de Plater, L., Guyader, C., De Pinieux, G., Judde, J.G., et al. (2007). A new model of patient tumor-derived breast cancer xenografts for preclinical assays. *Clin. Cancer Res.* 13, 3989–3998.
- Martens, T., Laabs, Y., Günther, H.S., Kemming, D., Zhu, Z., Witte, L., Hagel, C., Westphal, M., and Lamszus, K. (2008). Inhibition of glioblastoma growth in a highly invasive nude mouse model can be achieved by targeting epidermal growth factor receptor but not vascular endothelial growth factor receptor-2. *Clin. Cancer Res.* 14, 5447–5458.
- Nicholas, M.K., Lukas, R.V., Chmura, S., Yamini, B., Lesniak, M., and Pytel, P. (2011). Molecular heterogeneity in glioblastoma: therapeutic opportunities and challenges. *Semin. Oncol.* 38, 243–253.
- Phillips, H.S., Kharbanda, S., Chen, R., Forrest, W.F., Soriano, R.H., Wu, T.D., Misra, A., Nigro, J.M., Colman, H., Soroceanu, L., et al. (2006). Molecular subclasses of high-grade glioma predict prognosis, delineate a pattern of disease progression, and resemble stages in neurogenesis. *Cancer Cell* 9, 157–173.
- Pollard, S.M., Yoshikawa, K., Clarke, I.D., Danovi, D., Stricker, S., Russell, R., Bayani, J., Head, R., Lee, M., Bernstein, M., et al. (2009). Glioma stem cell lines expanded in adherent culture have tumor-specific phenotypes and are suitable for chemical and genetic screens. *Cell Stem Cell* 4, 568–580.
- Rubio-Viqueira, B., Jimeno, A., Cusatis, G., Zhang, X., Iacobuzio-Donahue, C., Karikari, C., Shi, C., Danenberg, K., Danenberg, P.V., Kuramochi, H., et al. (2006). An in vivo platform for translational drug development in pancreatic cancer. *Clin. Cancer Res.* 12, 4652–4661.
- Sausville, E.A., and Burger, A.M. (2006). Contributions of human tumor xenografts to anticancer drug development. *Cancer Res.* 66, 3351–3354, discussion 3354.
- Son, M.J., Woolard, K., Nam, D.H., Lee, J., and Fine, H.A. (2009). SSEA-1 is an enrichment marker for tumor-initiating cells in human glioblastoma. *Cell Stem Cell* 4, 440–452.
- Stupp, R., Mason, W.P., van den Bent, M.J., Weller, M., Fisher, B., Taphoorn, M.J., Belanger, K., Brandes, A.A., Marosi, C., Bogdahn, U., et al.; European Organisation for Research and Treatment of Cancer Brain Tumor and Radiotherapy Groups; National Cancer Institute of Canada Clinical Trials Group. (2005). Radiotherapy plus concomitant and adjuvant temozolomide for glioblastoma. *N. Engl. J. Med.* 352, 987–996.
- Subramanian, A., Tamayo, P., Mootha, V.K., Mukherjee, S., Ebert, B.L., Gillette, M.A., Paulovich, A., Pomeroy, S.L., Golub, T.R., Lander, E.S., and Mesirov, J.P. (2005). Gene set enrichment analysis: a knowledge-based approach for interpreting genome-wide expression profiles. *Proc. Natl. Acad. Sci. USA* 102, 15545–15550.
- Taillandier, L., Antunes, L., and Angioi-Duprez, K.S. (2003). Models for neuro-oncological preclinical studies: solid orthotopic and heterotopic grafts of human gliomas into nude mice. *J. Neurosci. Methods* 125, 147–157.
- Verhaak, R.G., Hoadley, K.A., Purdom, E., Wang, V., Qi, Y., Wilkerson, M.D., Miller, C.R., Ding, L., Golub, T., Mesirov, J.P., et al.; Cancer Genome Atlas Research Network. (2010). Integrated genomic analysis identifies clinically relevant subtypes of glioblastoma characterized by abnormalities in PDGFRA, IDH1, EGFR, and NF1. *Cancer Cell* 17, 98–110.
- Wang, J., Miletic, H., Sakariassen, P.Ø., Huszthy, P.C., Jacobsen, H., Brekkå, N., Li, X., Zhao, P., Mørk, S., Chekenya, M., et al. (2009). A reproducible brain tumour model established from human glioblastoma biopsies. *BMC Cancer* 9, 465.
- Xie, Q., Thompson, R., Hardy, K., DeCamp, L., Berghuis, B., Sigler, R., Knudsen, B., Cottingham, S., Zhao, P., Dykema, K., et al. (2008). A highly invasive human glioblastoma pre-clinical model for testing therapeutics. *J. Transl. Med.* 6, 77.
- Yang, S.H., Kim, Y.H., Kim, J.W., Park, C.K., Park, S.H., and Jung, H.W. (2009). Methylation status of the O6-methylguanine-deoxyribonucleic acid methyltransferase gene promoter in World Health Organization grade III gliomas. *J Korean Neurosurg. Soc.* 46, 385–388.
- Yi, D., Hua, T.X., and Lin, H.Y. (2011). EGFR gene overexpression retained in an invasive xenograft model by solid orthotopic transplantation of human glioblastoma multiforme into nude mice. *Cancer Invest.* 29, 229–239.
- Zhuo, Y., Wu, Y., Guo, A., Chen, S., and Su, J. (2010). [Establishment and its biological characteristics of patient-derived lung cancer xenograft models]. *Zhongguo. Fei. Ai. Za. Zhi.* 13, 568–574.